Cryogenics 70 (2015) 1–8

Contents lists available at ScienceDirect

Cryogenics

journal homepage: www.elsevier.com/locate/cryogenics

New application of plate–fin heat exchanger with regenerative cryocoolers

Ho-Myung Chang *, Kyung Hyun Gwak

Hong Ik University, Seoul 121-791, Republic of Korea

ARTICLE INFO

Article history:
Received 6 January 2015
Received in revised form 11 March 2015
Accepted 18 April 2015
Available online 27 April 2015

Keywords:
Heat exchanger
Plate–fin
GM cryocooler
Liquid nitrogen

ABSTRACT

A design idea is newly proposed and investigated for the application of plate–fin heat exchanger (PFHX) with regenerative cryocoolers. The role of this heat exchanger is to effectively absorb heat from the stream of coolant and deliver it to the cold-head of a cryocooler. While various types of tubular HX's have been developed so far, a small PFHX could be more useful for this purpose by taking advantage of compactness and design flexibility. In order to confirm the feasibility and effectiveness, a prototype of aluminum-brazed PFHX is designed, fabricated, and tested with a single-stage GM cryocooler in experiments for subcooling liquid nitrogen from 78 K to 65–70 K. The results show that the PFHX is 30–50% more effective in cooling rate than the tubular HX's. Several potential applications of PFHX are presented and discussed with specific design concepts.

1. Introduction

Regenerative cryocoolers are conveniently used in many cryogenic systems, where the refrigeration load is relatively small. A number of cryocooler models are available in market as Stirling, GM (Gifford–McMahon), or pulse tube cycle. Even though the operating principle of the refrigeration cycles is different each other [1,2], every regenerative cryocooler has the coldest cooling part in common as a cylindrical head surface called "cold-head". Since the diameter of cold-head is small (typically less than 120 mm), the effective cooling area is quite limited, which often becomes a major constraint in efficient thermal design.

A heat exchanger (HX) is employed to effectively absorb heat from a stream of coolant (such as liquid nitrogen or gaseous helium) and deliver the thermal load to the cold-head. Various types of tubular HX's have been developed for different applications so far. Yoshida et al. [3] and Suzuki et al. [4] used "tube-on-cylinder" HX's for HTS power systems as illustrated in Fig. 1(a). Liquid nitrogen is pumped and subcooled from 78 K to 65–70 K through two HX's attached to two units of GM coolers. The HX is composed of a thick cylindrical cup (upside down) as extended surface, on which a tube is spirally wound and brazed. Recently, Chang and Ryu [5] performed an experiment with different sizes of tubular HX's and also presented an analytical model to show that there exists an optimal size to maximize the cooling rate for a given unit of cryocooler.

A similar type of tubular HX was used also in GM–JT (Gifford–McMahon/Joule–Thomson) systems [6–9] for 4.2 K refrigeration, as shown in Fig. 1(b). The high-pressure helium stream of JT circuit is pre-cooled through spirally wound tubes at the cold-heads of two-stage GM cooler. In some cases, a finned-tube has been used in order to augment the external heat transfer. Similar HX's were used with GM cryocoolers for the cooling of HTS rotating machinery and superconducting magnetic energy storage (SMES) application. Since compactness is a major design factor in HTS motors for shipboard application [10], the cooling temperature of HTS windings is as low as 20–30 K [11], and a tubular HX was used as thermal interface between multiple units of GM coolers and circulating helium gas. In a recently developed SMES system [12], HTS windings were also cooled at 20 K by circular aluminum plates, having an internal hole through which gaseous helium is forced to flow. The thermal load is carried by helium to the cold-head of cryocooler, where a tubular HX was used as well.

Plate–fin heat exchanger (PFHX) is another (far different) type of heat exchanger, being also widely used in large-scale cryogenic refrigeration and liquefaction systems. It is made with multiple layers of corrugated aluminum sheets separated by flat plates to create a series of finned chambers. The primary advantage of PFHX is compactness and design flexibility. The surface area per unit volume is much greater (over ten times) than that of conventional shell-and-tube heat exchangers [13]. PFHX is easily designed in a variety of configurations, such as counter-flow, parallel flow,

* Corresponding author. Tel.: +82 2 320 1675.
E-mail address: hmchang@hongik.ac.kr (H.-M. Chang).

http://dx.doi.org/10.1016/j.cryogenics.2015.04.005
0011-2275/

Nomenclature

C_P	specific heat of liquid nitrogen
d	hydraulic diameter
H	heat exchanger effective height
h	heat transfer coefficient
k	thermal conductivity
L	heat exchanger length
l	fin height
$\dot{m}$	mass flow rate
m_{LN}	mass of liquid nitrogen container
Nu	Nusselt number
q	cooling rate
T	temperature
t	time
w	fin pitch
z	vertical distance from bottom

Greek letters

δ	thickness of fin or plate
η_f	fin efficiency

Subscripts

1, 2, 3, ...	layer number of PFHX
e	exit
i	inlet
j	summation index of multi-stream
PFHX	plate–fin heat exchanger
w	side wall

cross flow, multi-pass or multi-stream HX's. [14,15]. On the other hand, the axial conduction through the aluminum plates could be an obstacle, if a large temperature gradient is required for compact cryogenic design.

In this study, it is proposed to apply a PFHX to various cryogenic systems where regenerative cryocoolers are used. This idea is motivated by an intuition that the axial conduction could be positively utilized, while still taking advantage of compactness and design flexibility. The direct combination of PFHX and regenerative cryocooler has never been reported, as far as the authors are aware. In order to confirm the feasibility of the proposed idea, it is intended to design, fabricate, and experimentally test a prototype of PFHX with a commercial GM cryocooler. In addition, a variety of potential application schemes of PFHX's are pursued.

2. Design and fabrication of PFHX

A plate–fin HX is designed for use with a single-stage GM cryocooler (Sumitomo Heavy Industry model RDK-500B [16,17]), as graphically shown in Fig. 2. The top portion of two rectangular side plates is bent by 90° so that the "wing-shaped" flanges can be served for bolt-joint with the cold-head. Out of 8 threaded holes evenly spaced on the bottom circle (108 mm diameter) of cold-head, 6 holes (3 holes with each plate) are used for assembly. The contact area between the cold-head and the PFHX is approximately 5500 mm^2 (61% area of the circle), which is the sum of two "D-shaped" circular segments. The top surface of flanges is machined and polished for a good thermal contact. The side plates will play an important role of thermal conductor that delivers heat from the streams in PFHX to the cold-head of cryocooler.

The number of layers between two side plates is seven, which is determined by the geometric constraint of cold-head. The seven layers are classified as two groups: odd-numbered (1, 3, 5, 7) and even-numbered (2, 4, 6) layers, which will be called "O-layers" and "E-layers", respectively. As shown in Fig. 3, the inlet/exit ports are located at left-top and right-bottom for O-layers and at right-top and left-bottom for E-layers. The two groups of layers can be used in parallel flow or counter-flow, as necessary. The custom-ordered PFHX is fabricated by a manufacturer in Korea. The specifications of prototype PHHX are listed in Table 1. Material of all parts including corrugated fins, sheets/plates, and inlet/exit ports is aluminum, and the cross-section of a flow channel is 1.3 mm × 3 mm ($w \times l$). Fig. 3 is the photographs of layer-by-layer views, stacked layers, and final product of the prototype PFHX.

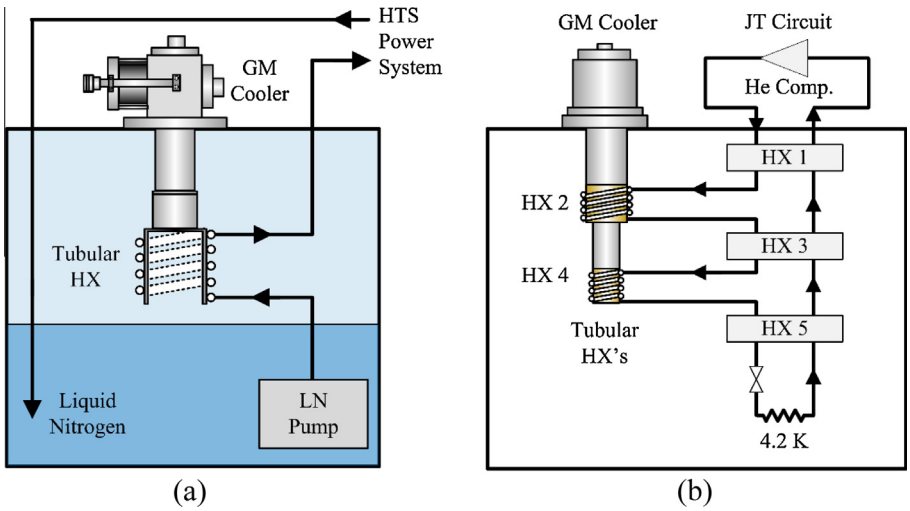

Fig. 1. Existing applications of tubular HX's with regenerative cryocoolers. (a) Liquid-nitrogen HX with single-stage GM cooler. (b) Helium HX for GM–JT refrigeration at 4.2 K.

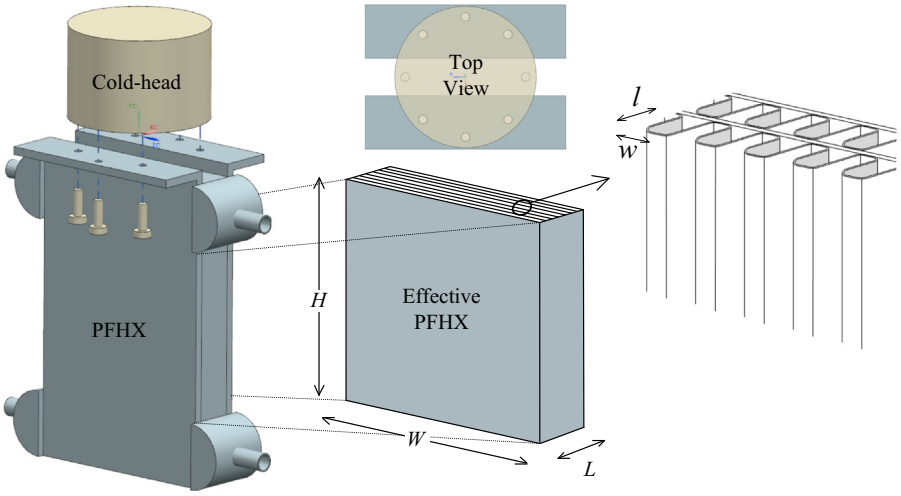

Fig. 2. Graphical representation of design concept for PFHX assembly with cold-head and geometric notation for dimension of PFHX and fins.

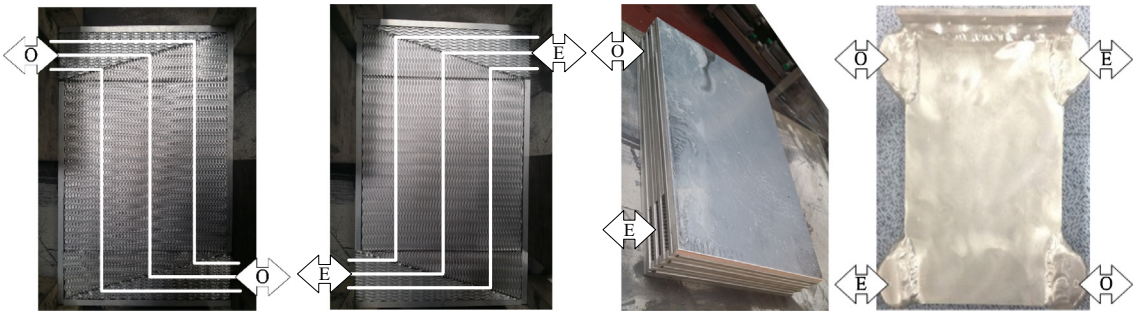

Fig. 3. Photographs of layer-by-layer view (O-layer and E-layer with a few streamlines by white lines), stacked layers, and final product of prototype PFHX.

Table 1
Specifications of prototype PFHX.

Number of layers	O-layers	4 (1, 3, 5, 7)
	E-layers	3 (2, 4, 6)
Total length	L	40 mm
Total height		230 mm
Effective height	H	160 mm
Total width	W	150 mm
Fin type		Wavy fins
Fin thickness	δ	0.1 mm
Fin height	l	3.0 mm
Fin pitch	w	1.3 mm
Parting sheet thickness		1.0 mm
Side bar thickness		5.0 mm
Side plate thickness	δ_w	5.0 mm
Inlet/exit port diameter		12.7 mm

3. Experiment and analysis with liquid nitrogen

3.1. Experimental set-up and procedure

Fig. 4 is the schematic overview of experimental apparatus to verify the performance of prototype PFHX in subcooling liquid nitrogen (LN). As mentioned with Fig. 1, subcooled LN is a common coolant for HTS power systems, such as HTS transmission cables, HTS fault current limiters, and HTS power transformers. The single-stage GM cryocooler (SHI model RDK-500B) is installed on the top plate of a cryostat, and the prototype PFHX is bolt-jointed to its cold-head. The O-layers and E-layers are arranged as parallel flow for this LN experiment, as schematically shown in Fig. 4. Liquid from a pressurized container is supplied to the PFHX through a long (15 m) pre-cooling tube submerged in LN pool. Since the cryostat is maintained at atmospheric pressure, the LN pool temperature is close to 77.4 K at all times. The LN stream at the inlet is clearly in

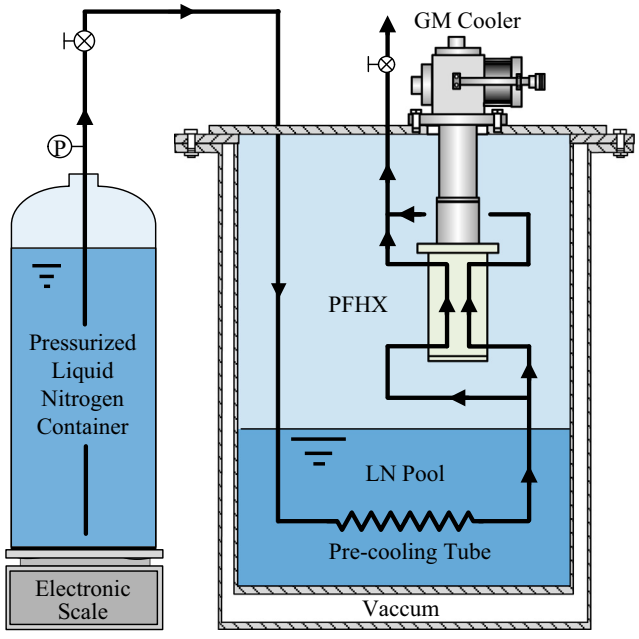

Fig. 4. Schematic overview of experimental apparatus.

liquid phase, because the liquid pressure in the PFHX is 350–400 kPa (the corresponding boiling temperature is 89.7–91.3 K) and the inlet temperature is around 77.8 K. Depending on the flow rate and effectiveness of the PFHX, the LN stream is further sub-cooled at the exit. The LN cooling rate at the PFHX is calculated as

$$q_{PFHX} = \dot{m} C_P (T_i - T_e) \tag{1}$$

where $\dot{m}$ and C_P are the flow rate and specific heat (2.02 J/g K) of LN, respectively. Since T_i is constant, the cooling at the PFHX is more effective if $\dot{m}$ is larger or T_e is lower. Experiment is performed by varying $\dot{m}$ so as to have T_e in the range of 65–70 K. The external surface of cold body (including the cold-head, PFHX, and connecting tubes) is wrapped with foam insulation. The cold body is also covered with a plastic bag in order to prevent any condensation of boil-off vapor in the cryostat. Fig. 5 is a photograph of top-plate assembly including the GM cryocooler, radiation shield, PFHX, and pre-cooling tube (hidden inside the cryostat).

Temperature is measured at the cold-head, inlet/exit tubes of PFHX, and several locations of side plates with silicon diode sensors (Lakeshore DT-670-SD). The sensors are attached on the surface with cryogenic epoxy or varnish, and temperature is recorded with two units of data logger (Lakeshore Temperature Monitor 218).

There are a few possible ways to measure the flow rate of LN. One is to use a cryogenic liquid flow-meter at the entrance of PFHX, but a vortex or turbine type of flow-meter is not readily available for the small flow rates. Another way is to use a standard gas flow-meter at room temperature, as executed in [5]. For this measurement, a long warm-up passage is necessary between the cryostat and the flow-meter, which makes the flow control unstable and difficult. A simpler way is taken here to use an electronic scale (maximum 300 kg with accuracy of 0.005 kg) for the LN container mass (m_{LN}) and estimate the flow rate by numerical differentiation.

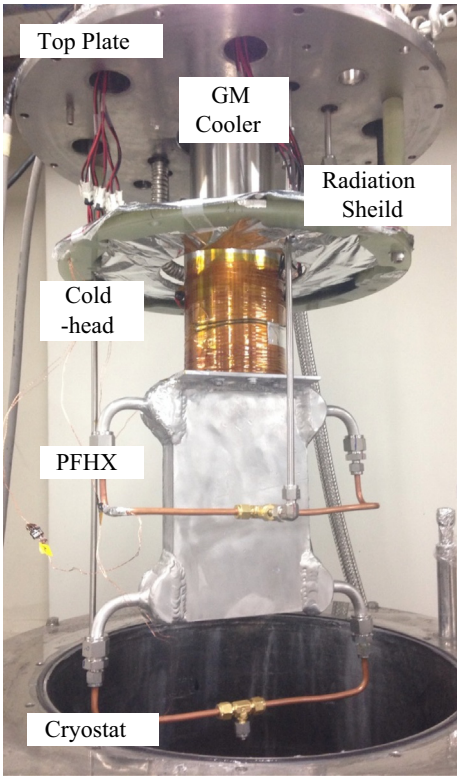

Fig. 5. Photograph of top-plate assembly.

$$\dot{m} = -\frac{dm_{LN}}{dt} \approx \frac{m_{LN}(t - \Delta t) - m_{LN}(t + \Delta t)}{2\Delta t} \tag{2}$$

as satisfactorily worked in Chang and Gwak [14]. This value is accurate and independent of the sampling time (Δt), since only a "steady" flow rate is needed in this experiment. The LN flow can be easily set at any desired level in the range of 6–12 g/s by regulating a valve at the exit, where LN is discharged to atmosphere.

Fig. 6 shows an example of measured time history of LN flow rate and temperature at various locations. The inlet temperature is maintained at 77.7–77.9 K at all times. As the LN flow rate increases stepwise from 8.2 g/s to 11.3 g/s, the exit temperature also increases with a time-leg in the range between 66.9 K and 69.1 K. It is noted that the exit temperature is measured at the mixed stream flowing out of 7 layers (i.e. both O-layers and E-layers) and the flow rate is also the sum of flow rates in 7 layers. The dotted line indicates the freezing temperature of LN (63.3 K), below which the flow passage may shrink by freeze-out [14].

The effective cooling rate of the LN streams can be calculated by Eq. (1). As the inlet temperature is 77.8 K at all times, the LN cooling rate is around 179–190 W in this experiment. On the other hand, the refrigeration capacity of this cryocooler is approximately 190–205 W at 52–54 K from the experiments by Chang and Lee [17]. The difference between refrigeration capacity and effective cooling is less than 15 W, which is the estimated background (or passive) heat load of this experimental system, including the conduction through insulation and the radiation on the cold parts. It is believed therefore that over 90% of the refrigeration power has been utilized to cool the LN streams with this PFHX. Since the temperature difference between the cold-head and PFHX flanges is approximately 2.2–2.4 K, the estimated contact resistance is around 7×10^{-5} m^2 K/W, which is comparable with the reference data on aluminum–copper interface in vacuum ($1–5 \times 10^{-5}$ m^2 K/W) [18]. In practical systems, the thermal contact can be considerably improved by reducing the surface roughness of flanges and/or filling the gap with soft metal such as indium.

The thermal performance of entire cooling system, including the cold-head and PFHX, is determined by three factors: (1) HX effectiveness, (2) thermal contact between HX and cold-head, (3) refrigeration capacity of cryocooler. In the previous study on tubular HX's [5], the effect of these factors was quantitatively taken into consideration with "thermal resistance model". In this case, however, the same model is not readily applicable, because the temperature distribution is not one-dimensional near the top of PFHX. As described in next section, the wall temperature is expected to be one-dimensional (i.e. dependent only on its height) from the bottom to z = 160 mm, but significantly vary across the width as well at the exit part (z > 160 mm).

3.2. Numerical analysis

A simple one-dimensional model is considered here for 2 side walls and 7 streams with the notations in Fig. 7, even though the actual thermal phenomena in PFHX may be complicated in general [19–22]. By symmetry, it is assumed that two wall temperatures are same and

$$T_1(z) = T_7(z),\ T_2(z) = T_6(z),\ T_3(z) = T_5(z) \tag{3}$$

The vertical coordinate, z is the distance from the bottom of effective HX (excluding the inlet and exit parts). The unknown variables are now reduced to $T_w(z)$, $T_1(z)$, $T_2(z)$, $T_3(z)$, $T_4(z)$, and the temperature distribution is determined by a set of energy balance equations

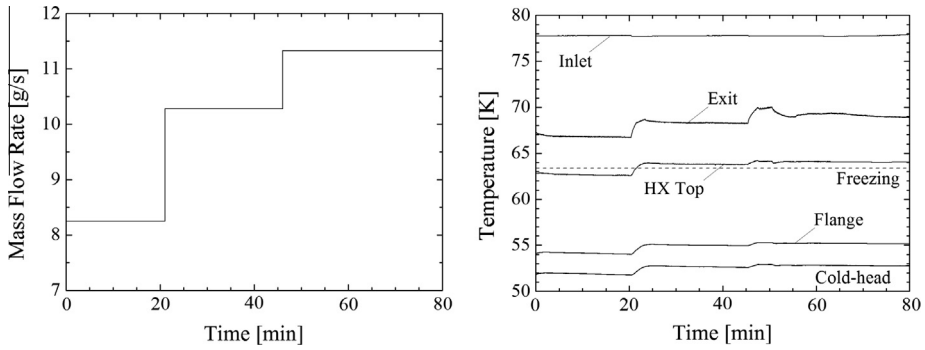

Fig. 6. Measured time history of LN flow rate and temperature at inlet, exit, top, flange, and cold-head.

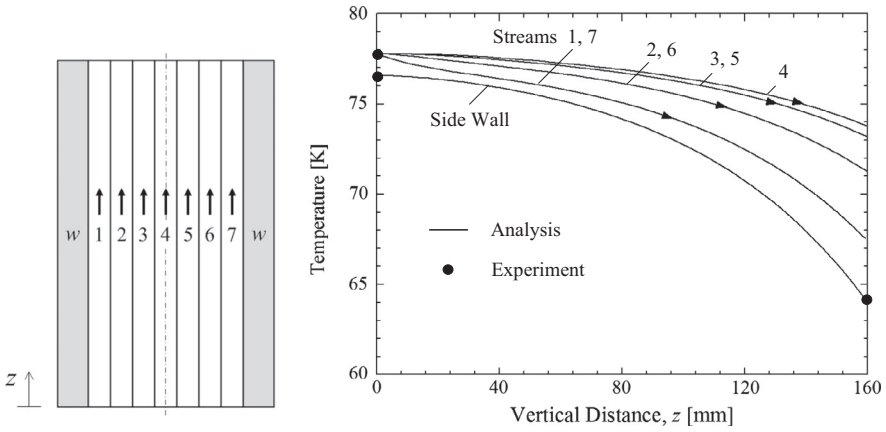

Fig. 7. Schematic cross-section of PFHX and calculated temperature distributions of side wall and LN streams.

$$-k_w\delta_w W\frac{d^2T_w}{dz^2}=hW\left(1+\frac{\eta_f l}{w}\right)(T_1-T_w) \tag{4}$$

$$\dot{m}_1C_P\frac{dT_1}{dz}=\frac{hW}{2}\left(1+\frac{\eta_f l}{w}\right)(T_2-T_1)-\frac{hW}{2}\left(1+\frac{\eta_f l}{w}\right)(T_1-T_w) \tag{5}$$

$$\dot{m}_2C_P\frac{dT_2}{dz}=\frac{hW}{2}\left(1+\frac{\eta_f l}{w}\right)(T_3-T_2)-\frac{hW}{2}\left(1+\frac{\eta_f l}{w}\right)(T_2-T_1) \tag{6}$$

$$\dot{m}_3C_P\frac{dT_3}{dz}=\frac{hW}{2}\left(1+\frac{\eta_f l}{w}\right)(T_4-T_3)-\frac{hW}{2}\left(1+\frac{\eta_f l}{w}\right)(T_3-T_2) \tag{7}$$

$$\dot{m}_4C_P\frac{dT_4}{dz}=-\frac{hW}{2}\left(1+\frac{\eta_f l}{w}\right)(T_4-T_3)-\frac{hW}{2}\left(1+\frac{\eta_f l}{w}\right)(T_4-T_5)=-hW\left(1+\frac{\eta_f l}{w}\right)(T_4-T_3) \tag{8}$$

where the parenthesis $(1+\eta_f l/w)$ accounts for the effect of prime surface (i.e. parting sheets) and fin surface in terms of fin efficiency [18]. In this PFHX, the fin efficiency is calculated as

$$\eta_f=\frac{\tanh\sqrt{l^2h/2k_w\delta}}{\sqrt{l^2h/2k_w\delta}} \tag{9}$$

because the fin is considered a straight rectangular fin of thickness δ and length $l/2$ (by symmetry) [23]. In Eqs. 5–8, the terms in right handed side are divided by 2, because the thermal resistance on both sides of a parting sheet should be taken into account. The heat transfer coefficient, h, is estimated with engineering correlations for fully developed flow in a rectangular channel.

$$h=\frac{k}{d}Nu_d \tag{10}$$

where k is the thermal conductivity of LN and d is the hydraulic diameter of a rectangular channel, defined as

$$d=\frac{2wl}{w+l} \tag{11}$$

The LN flow through this narrow passage (d = 1.80 mm as listed in Table 2) is laminar in all experimental conditions, thus Nu_d is given in the range of 3.6–4.3 [18] for the rectangular channel. The boundary conditions of Eqs. 4–8 are given as

$$\frac{dT_w(0)}{dz}=0,\ T_1(0)=T_2(0)=T_3(0)=T_4(0)=77.8\text{ K},\ T_w(H)=64.0\text{ K (from experiment)} \tag{12}$$

and it is assumed for simplicity that the mass flow rate of LN is evenly distributed for all streams. The equations are numerically solved with fourth-order Runge–Kutta integration and a shooting method. The exactness of numerical solution can be confirmed by the sum of integrated energy equations with boundary conditions (12).

Table 2
Values of properties and parameters used in calculation.

Specific heat of liquid nitrogen	C_P	2.01 J/g K
Thermal conductivity of liquid nitrogen	k	0.150 W/m K
Thermal conductivity of aluminum (3003)	k_w	140 W/m K
Hydraulic diameter	d	1.80 mm
Heat transfer coefficient	h	391 W/m^2 K
Fin efficiency	η_f	0.963
Mass flow rate in a layer	$\dot{m}_j$	1.61 g/s

$$-2k_w\delta_w W\frac{dT_w(H)}{dz}=\sum_{j=1}^{7}\dot{m}_j C_P\left[T_j(0)-T_j(H)\right] \quad (13)$$

The calculated temperature distributions of side wall and LN stream in 7 layers are plotted in Fig. 7 in comparison with the experimental data. The values of properties and parameters used in the calculation are listed in Table 2. The calculated $T_w(0)$ is in good agreement with the experimental value. Since there is no experimental information on respective 7 streams, the measured exit temperature (69.0 K) of mixed stream is compared with the average of calculated seven exit temperatures (71.0 K). A main reason for this difference is that the LN streams are rather actively cooled at the exit part above the effective PFHX (for $z > 160$ mm), where this one-dimensional model is not valid any more. Other reason may be the effect of non-uniform distribution of LN flow in 7 layers, which does not appear to be significant, as the flow resistance is nearly the same.

3.3. Results and discussion

Fig. 8 is the summary of experimental results as a plot of LN flow rate vs. exit temperature with the previous tubular HX data [5]. As the exit temperature increases over the range of 65–70 K, the LN flow rate increases almost linearly in this experiment. The cooling rate with PFHX is much greater than the previously reported values with tubular HX's.

To be exact, the experimental conditions are slightly different each other. The GM cooler is Cryomech AL300 in [5] and SHI RDK-500B in this study. These two coolers are, however, similar in the size of cold-head and the refrigeration capacity at working temperatures. The diameter of cold-head is 100 mm for AL300, and 108 mm for RDK-500B, but the actual contact area with HX is 7800 mm^2 and 5500 mm^2, respectively. The refrigeration capacity is approximately 200 W at 50 K for AL300, and 180 W at 50 K for RDK-500B. The coldhead of AL300 was rebuilt by the manufacturer after a few years of operation, but the RDK-500B is a newly developed model. The prototype PFHX is larger than the tubular HX's in overall size. It is recalled again that there exists an optimal size of tubular HX (118 mm diameter × 73 mm height) [5], which is comparable with the effective size (excluding the inlet and exit parts) of PFHX (40 mm × 150 mm × 160 mm). The inlet temperature of LN is 77.8 ± 0.2 K in both experiments. The liquid pressure varies over a range of 300–400 kPa, as the LN container pressure decreases, but the enthalpy of LN is almost independent of pressure in the experimental conditions. The tubular HX's are made of oxygen-free copper, while the PFHX is made of aluminum 3003. As a result, the metallic contact interfaces are copper–copper and copper–aluminum, respectively.

Overall, it can be stated that the PFHX is superior to tubular HX's in thermal performance. In this specific experiment, the prototype PFHX is 30–50% more effective in the cooling rate of LN. It is also noticeable that the merit of PFHX becomes greater as the flow rate increases, because the large surface area of compact HX becomes more useful. On the other hand, of course, the larger pressure drop should be considered as a common drawback of all compact HX's.

4. Other proposed applications

There are many potential application areas where the proposed PFHX can be effectively used with regenerative cryocoolers. As mentioned in Introduction, the existing tubular HX's may be replaced by properly designed PFHX's for HTS cables, fault current limiters, transformers, motors, SMES systems. Two specific application areas are proposed and discussed here for future development. The first is a cooling system for HTS wind turbine generators under active research. Over past decade, the feasibility of a 10 MW class turbine has been extensively studied with focus on offshore application [24–26]. Among different cryogenic cooling schemes, an on-board cooling system is illustrated in Fig. 9. Depending on the winding design, 3 or 4 units of GM cryocoolers are symmetrically mounted on the rotating cryostat in radial direction. On the cold-head of GM coolers, a PFHX can be used for effectively cooling the helium stream circulated by a centrifugal fan. The compactness and light weight of aluminum PFHX are significantly advantageous in this application.

Another new application of PFHX is proposed for GM–JT refrigeration at liquid-helium temperature. The GM–JT refrigeration is a combined system of GM cryocooler and JT circuit, which was developed in 1980s (before the advent of 4 K GM coolers) for a small load (1–2 W) at 4.2 K [6]. The GM–JT systems are still under use for applications with a cooling load of 2 W or larger [7–9]. Fig. 1(b) is a commercially available system with two-stage GM cooler, where the high-pressure stream is pre-cooled by two steps. The main reason why the capacity of existing GM–JT system is only 3–5 W at 4.2 K is that the cooling rate at the second (i.e. colder) stage is small and limited for all available GM cryocoolers. Recently state-of-the-art single-stage GM coolers with a greater capacity (over 20 W at 20 K) are released [27,28]. It is expected in combination with PFHX that the refrigeration capacity of GM–JT system could be considerably increased. As schematically

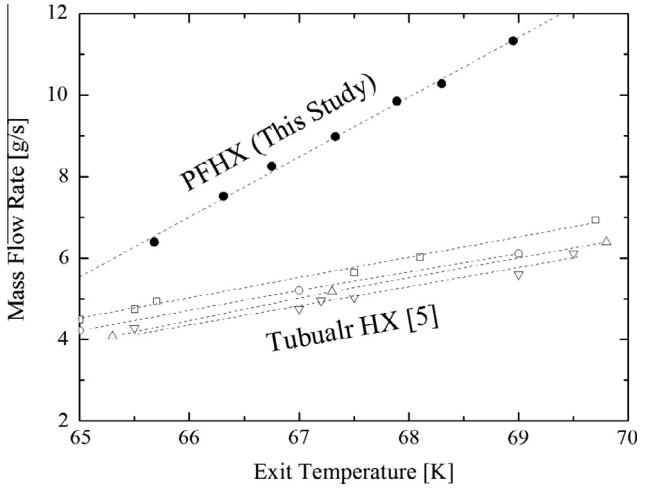

Fig. 8. Experimental results of LN flow rate as a function of exit temperature.

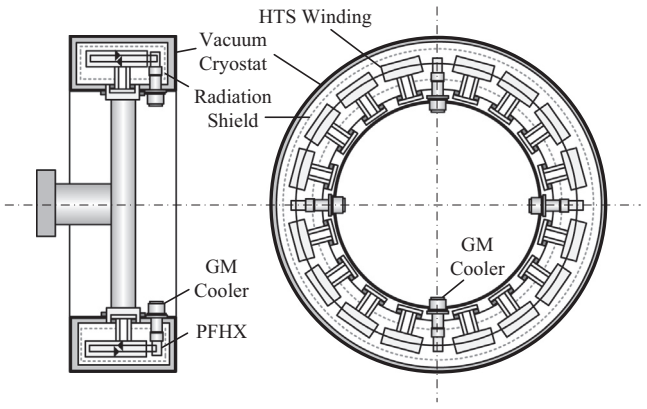

Fig. 9. Schematic diagram of proposed on-board cooling system with PFHX's and GM cryocoolers for 10 MW-class HTS wind turbine generator.

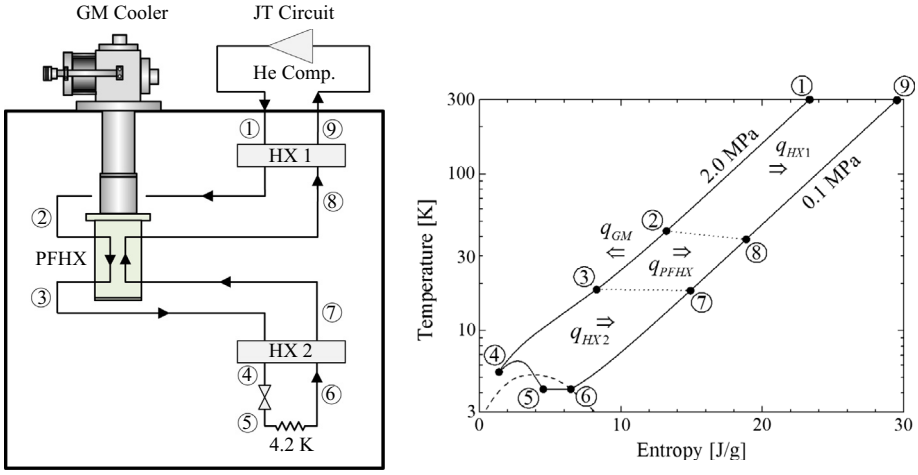

Fig. 10. Proposed GM–JT refrigeration system and simulated cycle on temperature–entropy diagram.

shown in Fig. 10, the PFHX is arranged as counter-flow of high-pressure and low-pressure streams so that the GM cooler may be in assistance to the unbalanced specific heats of two streams. Full details of this thermodynamic study are beyond the scope of this paper, but it is roughly estimated with commercial software (Aspen HYSYS) that the capacity can be as high as 10–12 W at 4.2 K as demonstrated in temperature–entropy diagram in Fig. 10. The PFHX is a key component that will enable this GM–JT refrigeration.

Finally, future work is recommended as next step, and a technical limit in the proposed applications is briefly mentioned. It is important to understand the detailed temperature distribution in PFHX for an accurate HX design. As noted above, the temperature distribution must be significantly two-dimensional due to the combination of a circular cold-head and a rectangular PFHX. Further study is recommended to elaborate and experimentally verify a design scheme that includes the geometric effect and wall conduction.

When compared with tubular HX's, PFHX's have a weakness in high-pressure applications, depending on the brazing and welding technique. A top PFHX manufacturer claims that the maximum design pressure of aluminum brazed PFHX is 11 MPa [15]. The operating pressure in the systems presented here is well below this limit, but other application areas (for example, a small scale liquefaction of hydrogen or natural gas) may be considered as well, if the required pressure is 10 MPa or less.

5. Summary and conclusion

The feasibility and effectiveness of PFHX is investigated for its practical application with regenerative cryocoolers. A prototype of aluminum-brazed PFHX is designed and successfully fabricated in a size and shape that can be directly bolt-jointed to the cold-head of a single-stage GM cryocooler. The thermal performance of the prototype is experimentally tested and analytically calculated on the process of continuously cooling a liquid-nitrogen stream from 78 K to 65–70 K. The results show that the PFHX is 30–50% more effective in the cooling rate than the conventional tubular HX's. It is concluded that PFHX is usefully applicable to a cryogenic cooling system with regenerative cryocoolers, still taking advantage of its compactness and design flexibility. In addition to the liquid-nitrogen systems for HTS power application, PFHX's can be extensively used in various helium systems, including HTS rotating machines, superconducting magnetic energy storage (SMES) magnets, and GM–JT refrigerators with a larger capacity.

Acknowledgments

This work was supported by a grant of the Power Generation & Electricity Delivery Program of the Korea Institute of Energy Technology Evaluation and Planning (KETEP) funded by the Ministry of Trade, Industry and Energy of Korean Government (No. 20141010502318). The authors wish to thank the Donghwa Entec Co. Ltd. (http://www.dh.co.kr/) for fabricating the prototype of plate–fin heat exchanger and the Cryogenics Group of Sumitomo Heavy Industries for leasing the GM cryocooler.

References

[1] Walker G. Cryocoolers, Part 1. New York: Plenum Press; 1983.
[2] Barron RF. Cryogenic systems. 2nd ed. New York: Oxford University Press; 1985.
[3] Yoshida S, Ohashi K, Umeno T, Suzuki Y, Kamioka Y, Kimura H, et al. 1 Atm subcooled liquid nitrogen cryogenic system with GM-refrigerator for a HTS power transformer. Adv Cryog Eng 2002;47:473–80.
[4] Suzuki Y, Yoshida S, Kamioka Y. Subcooled liquid nitrogen refrigerator for HTS power systems. Cryogenics 2003;43(10–11):597–602.
[5] Chang HM, Ryu SH. Heat exchanger for subcooling liquid nitrogen with a regenerative cryocooler. Cryogenics 2011;51:132–8.
[6] Longsworth RC. Cryostat with serviceable refrigerator. US Patent 4, 277, 949; 1981.
[7] Chang HM. Design of GM–JT refrigerators. Int J Air-Condition Refrig 1995;3:1–11.
[8] Jia LX, Wang L, Addessi L, Miglionico G, Martin D, Leskowicz J, et al. A five-watt G–M/J–T refrigerator for LHe target at BNL. Adv Cryog Eng 2002;47:776–81.
[9] Aoki K, Haruyama T, Makida Y, Araoka O, Kasami K, Takahashi T, et al. Development of new cooling system using GM/JT cryocoolers for the SKS magnet. Adv Cryog Eng 2008;53:349–56.
[10] Gamble B, Snitchler G, MacDonald T. Full power test of a 36.5 MW HTS propulsion motor. IEEE Trans Appl Supercond 2011;21:1083–8.
[11] Chang HM, Choi YS, Van Sciver SW. Optimization of operating temperature in cryocooled HTS magnets for compactness and efficiency. Cryogenics 2002;42:787–94.
[12] Nagaya S, Hirano N, Katagiri T, Tamada T, Shikimachi K, Iwatani Y, et al. The state of the art of the development of SMES for bridging instantaneous voltage dips in Japan. Cryogenics 2012;52:708–12.
[13] Barron RF. Cryogenic heat transfer. Philadelphia: Taylor & Francis; 1999.
[14] Chang HM, Gwak KH, Yang HS, Hwang SD. Cross-flow heat exchangers for anti-freezing of liquid nitrogen. Cryogenics 2013;57:122–8.
[15] Linde Engineering <http://www.linde-engineering.com/> [accessed March, 2015].
[16] Yamada K. Development of a large cooling capacity single stage GM cryocooler. Cryogenics 2014;63:110–3.
[17] Chang HM, Lee SI. Conduction-cooling system for superconducting magnets at 20–30 K. IEEE Trans Appl Supercond 2014;24:3800204.
[18] Incropera FP, DeWitt DP, Bergman TL, Lavine AS. Fundamentals of heat and mass transfer. 6th ed. Hoboken, NJ: John Wiley & Sons; 2007.

[19] Nellis GF. A heat exchanger model that includes axial conduction, parasitic heat loads, and property variations. Cryogenics 2003;43:523–8.
[20] Jung J, Jeong S. Effect of flow mal-distribution on effective NTU in multi-channel counter-flow heat exchanger of single body. Cryogenics 2007;47:232–42.
[21] Chang HM, Lim HS, Choe KH. Effect of multi-stream heat exchanger on performance of natural gas liquefaction with mixed refrigerant. Cryogenics 2012;52:642–7.
[22] Goyal M, Chakravarty A, Atrey MD. Two dimensional model for multistream plate fin heat exchangers. Cryogenics 2014;61:70–8.
[23] Chang HM, Chung MJ, Kim MJ, Park SB. Thermodynamic design of methane liquefaction system based on reversed-Brayton cycle. Cryogenics 2009;49:226–34.
[24] Abrahamsen AB, Mijatovic N, Seiler E, Zirngibl T, Træholt C, Nørgård PB, et al. Superconducting wind turbine generators. Supercond Sci Technol 2010;23:034019.
[25] Snitchler G, Gamble B, King C, Winn P. 10 MW class superconductor wind turbine generators. IEEE Trans Appl Supercond 2011;21:1089–92.
[26] Xu Y, Maki N, Izumi M. Study of key parameters and cryogenic vessel structure of 10-MW salient-pole wind turbine HTS generators. IEEE Trans Appl Supercond 2015;25:5200406.
[27] Cryogenics Group of Sumitomo Heavy Industries, Ltd <http://www.shicryogenics.com/> [accessed March, 2015].
[28] Cryoemch Inc. <http://www.cryomech.com/> [accessed March, 2015].